

HCN Observations of Dense Star-Forming Gas in High Redshift Galaxies

Yu Gao^{1,2}, Chris L. Carilli², Philip M. Solomon³, and Paul A. Vanden Bout⁴

ABSTRACT

We present here the sensitive HCN(1-0) observations made with the VLA of two submillimeter galaxies and two QSOs at high-redshift. HCN emission is the signature of dense molecular gas found in GMC cores, the actual sites of massive star formation. We have made the first detection of HCN in a submillimeter galaxy, SMM J16359+6612. The HCN emission is seen with a signal to noise ratio of 4σ and appears to be resolved as a double-source of $\lesssim 2''$ separation. Our new HCN observations, combined with previous HCN detections and upper limits, show that the FIR/HCN ratios in these high redshift sources lie systematically above the FIR/HCN correlation established for nearby galaxies by about a factor of 2. Even considering the scatter in the data and the presence of upper limits, this is an indication that the FIR/HCN ratios for the early Universe molecular emission line galaxies (EMGs) deviate from the correlation that fits Galactic giant molecular cloud cores, normal spirals, LIRGs, and ULIRGs. This indicates that the star formation rate per solar mass of dense molecular gas is higher in the high- z objects than in local galaxies including normal spirals LIRGs and ULIRGs. The limited HCN detections at high-redshift show that the HCN/CO ratios for the high- z objects are high and are comparable to those of the local ULIRGs rather than those of normal spirals. This indicates that EMGs have a high fraction of dense molecular gas compared to total molecular gas traced by CO emission.

Subject headings: galaxies: high-redshift — galaxies: starburst — infrared: galaxies — galaxies: ISM — galaxies: formation — ISM: molecules

¹Purple Mountain Observatory, Chinese Academy of Sciences (CAS), 2 West Beijing Road, Nanjing 210008, P.R. China; and National Astronomical Observatories, CAS, Beijing, P.R. China; yugao@pmo.ac.cn, ygao@nrao.edu

²National Radio Astronomy Observatory, Socorro, NM 87801, USA; ccarilli@nrao.edu

³Department of Physics & Astronomy, SUNY at Stony Brook, Stony Brook, NY 11794, USA; philip.solomon@sunysb.edu

⁴National Radio Astronomy Observatory, Charlottesville, VA 22903, USA; pvandenb@nrao.edu

1. Introduction

A molecule whose emission line luminosity is linearly related to the rate of star formation in a galaxy would be useful to the study of star formation and the evolution of galaxies since the emission can be used to directly and simply relate the star formation rate to physical properties of the ISM. The dust continuum emission in the far-infrared (FIR), re-radiated from dust heated by UV radiation from young massive stars, is a good indicator of the actual star formation rate. A molecular line tracer of star formation can be imaged at sub-arcsecond resolution and analyzed for the morphology and kinematics of the star-forming gas, whereas measurements of the FIR lack comparable spatial resolution.

Emission in the rotational lines of carbon monoxide is the cardinal indicator of the presence of molecular gas in galaxies, seen from the interstellar medium of the Milky Way to quasars at redshifts up to $z \sim 6$ (see Solomon and Vanden Bout 2005, for a review of the properties of the ~ 40 galaxies with CO emission detected at $z \geq 1$). CO emission is strong from star-forming giant molecular clouds (GMCs) in the Galaxy and external galaxies. And the FIR luminosity, a measure of the star formation rate, is directly proportional to CO luminosity for GMCs and normal spirals, but increases more rapidly than linearly with CO luminosity for luminous and ultraluminous infrared galaxies (LIRGs & ULIRGs, see Sanders and Mirabel 1996). Gao and Solomon (2004a, hereafter GS04a) find a slope of 1.7 over 3 orders of magnitude in luminosity for the $L_{\text{IR}} - L'_{\text{CO}}$ correlation including all of the CO observations of ULIRGs from Solomon et al. (1997). Thus for extreme starbursts such as ULIRGS the star formation rate per solar mass of total molecular gas traced by CO, a measure of the star formation efficiency, is much higher than for normal spirals.

In contrast to the FIR–CO correlation, the FIR–HCN correlation is a linear relation over three decades in HCN luminosity from normal spirals to ULIRGs (GS04a). This is based upon the HCN survey of 65 galaxies, including nearly 10 ULIRGs and more than 20 LIRGs (Gao & Solomon 2004b; Solomon, Downes, and Radford 1992). Indeed, Wu et al. (2005) have shown that the FIR–HCN correlation for galaxies extends down to individual dense cores in the star-forming GMCs in the Milky Way, spanning over eight decades in HCN luminosity. The key point is that HCN emission traces the gas actually undergoing star formation which is ~ 100 times denser than that traced by CO and the star formation rate is linearly proportional to the mass of dense gas with approximately $n(\text{H}_2) \gtrsim 3 \times 10^4 \text{ cm}^{-3}$ (Solomon, Downes, & Radford 1992; GS04a) The work reported here addresses the question of whether this linear FIR–HCN correlation, well-established for galaxies with redshifts $z < 0.1$, extends to EMGs at high- z .

Previous to this work, there were four high- z detections of HCN (Solomon et al. 2003; Vanden Bout et al. 2004; Carilli et al. 2005; Wagg et al. 2005) together with upper limits to

five others (Isaak et al. 2004; Carilli et al. 2005; Greve et al. 2006). The FIR/HCN ratios for these galaxies are all systematically offset from an extrapolation of the FIR–HCN relation for nearby normal spirals, LIRGs, and ULIRGs. Because an accurate molecular line tracer of star formation in EMGs is of great interest, it is important to know whether the EMGs truly lie above the FIR–HCN correlation observed for $z < 0.1$ or not. The four high- z detections and upper limits on 5 others lie at the limits of current telescope capabilities and the error bars can only be reduced with great expenditure of integration time. In addition, all four HCN detections at high redshift are quasars where the dust-enshrouded AGN contribution to the FIR emission could be significant. We attempted to increase the number of high- z HCN detections by observing two submillimeter galaxies, neither with an embedded AGN, and two more quasars with known strong CO emission.

2. Observations and Results

The galaxies selected for HCN(1-0), rest frequency $\nu=88.63185$ GHz, observations were four EMGs from the compilation of Solomon and Vanden Bout (2005) that had the strongest CO emission following that of those previously detected in HCN emission. In addition, their redshifted HCN lines fell into an observing band of the Very Large Array (VLA)⁵. The observations were carried out in the D configuration of the VLA in 2005 October and December for a total of 54 hours. A summary of the sources, observing times and observed frequencies is given in Table 1.

The lowest redshift source in our sample, a submillimeter (SMG) galaxy, SMM J02396-0134 at $z = 1.062$, was observed with the VLA 40-50 GHz receiver system in the 50 MHz continuum mode, which has two intermediate frequencies (IFs) of two polarizations each. Observations were made with two IF settings to provide the bandwidth required to cover the expected HCN line, as the CO line width is over 700 km s^{-1} broad. This provided four independent channels of 350 km s^{-1} each, two covering the expected HCN line and one each above and below the HCN line for a measurement of the continuum.

The redshifted HCN lines for other three sources fell in the VLA 21-25 GHz receiver system. These sources have CO line widths from 340 to 500 km s^{-1} (25 to 37 MHz). We observed these sources in the VLA 2AC mode with 7 channels of width 3.125 MHz (40 km s^{-1}) in each of the consecutive IF pair, providing a total of $\sim 550 \text{ km s}^{-1}$ velocity coverage. Standard VLA data reductions were performed in AIPS. And HCN channel maps were

⁵The Very Large Array is a facility of the National Radio Astronomy Observatory, operated by Associated Universities, Inc., under a cooperative agreement with the National Science Foundation.

obtained for each target with the AIPS task ‘imagr’. A summary of the observations and results is given in Table 2.

No significant HCN emission was seen in any of the targets except for the weak line at 4σ in SMM J16359+6612 (hereafter J16359), the other SMG in the sample. We obtained the velocity-integrated moment-zero map for each target by integrating over the channel maps covering the expected HCN line width, assumed to be the same as that of CO, leaving out the edge channels. The SMG J16359 shows weak but significant HCN emission at the strongest CO position (Fig. 1). The rms noise levels from these moment-zero maps were used to calculate the 3σ upper limits to the velocity-integrated HCN flux in the three undetected sources.

2.1. HCN(1-0) Emission in SMM J16359+6612

Figure 1 presents the HCN image of J16359. The SMG J16359 has three widely separated lensed components detected in CO (Kneib et al. 2005). We see a weak HCN signal at 3σ in the strongest of these CO lens components. To increase the signal-to-noise ratio, we extracted three HCN images of size $\sim 0.54'$ centered at the centroids (crosses) of each of the three CO lensed image components in Fig. 1. The inset image is a weighted average of these three HCN images. The (weighted) average HCN image shows a 4σ signal at the strongest CO position. This HCN source is barely resolved as a double source with a separation of $\lesssim 2''$. There is also a 3σ HCN signal $16''$ NE at the location of the second strongest CO lens component.

The reality of this tentative HCN detection in the component-averaged image of J16359 is further supported by the following features evident in the CO and HCN morphologies/kinematics:

1. The HCN emission maxima ($\geq 3\sigma$) are exactly at the centroids of the two strongest lensed CO components. And the strongest CO centroid is located in the middle of the double HCN components separated by $\lesssim 2''$.

2. The location, orientation, and separation of the HCN double-source are also consistent with those of inferred CO kinematics/morphology though the CO emission is spatially unresolved. They are also possibly associated with the optical features both spatially and kinematically (Kneib et al. 2005).

3. Further indirect evidence for a merger origin of J16359 has been summarized by Weiß et al. (2005). Although high resolution CO and high sensitivity HCN imaging is

required to directly reveal the putative merging morphology (or extended ~ 2 kpc edge-on dense gas ring/disk), the stacked HCN image provides the first direct evidence of a double-source in dense star-forming gas. We note that a double-source distribution in a lens image needs not imply the same distribution in the original object.

2.2. FIR–HCN Correlation in High-redshift Galaxies

Combining all HCN observations at high-redshift, including upper limits, yields a total of five HCN detections and eight upper limits, shown in Table 3. This sample contains four SMGs. We note that all of the HCN luminosities in Table 3 are for the (1-0) line.

HCN luminosities are calculated (Solomon et al. 2003) from $L'_{\text{HCN}} = 4.1 \times 10^3 S_{\text{HCN}} \Delta v (1+z)^{-1} D_L^2$, in $\text{K km s}^{-1} \text{pc}^2$, where $S_{\text{HCN}} \Delta v$ is the velocity integrated HCN line flux in Jy km s^{-1} , and D_L is the luminosity distance in Mpc. The HCN, CO, and FIR luminosities for our sample, are given in Table 3, together with the lens magnification that was assumed in correcting apparent to intrinsic luminosities.

In Figures 2-4 we show plots of FIR vs. HCN luminosity, the FIR/CO ratio vs. the HCN/CO luminosity ratio, and FIR luminosity vs. the HCN/CO ratio, respectively, for the 13 high- z galaxies of Table 3 together with those of a sample of 65 galaxies from the local HCN survey (GS04a).

3. Discussion

The five measurements and eight upper-limits to the HCN luminosities in the high- z EMGs shown in Figures 2 and 3, have systematically somewhat larger FIR luminosities than predicted by an extrapolation of the correlation that applies to local normal spirals, LIRGs, and ULIRGs. This hints at a slight deviation from linearity above a FIR luminosity $L_{\text{FIR}} > 2.5 \times 10^{12} L_{\odot}$ that is similar to the much larger non-linearity of the FIR–CO correlation particularly for LIRGs and ULIRGs with $L_{\text{FIR}} > 1 \times 10^{11} L_{\odot}$.

The local sample has an average ratio $L_{\text{FIR}}/L'_{\text{HCN}} = 750 L_{\odot} / \text{K km s}^{-1} \text{pc}^2$ for all 65 galaxies over a range of luminosity from 2×10^9 to $2 \times 10^{12} L_{\odot}$. The ULIRGs in the sample which have FIR luminosities $L_{\text{FIR}} > 7 \times 10^{11} L_{\odot}$ ($L_{\text{IR}} > 9 \times 10^{11} L_{\odot}$), have an average ratio of 880 with a 1σ dispersion of $(+330, -250) L_{\odot} / \text{K km s}^{-1} \text{pc}^2$. These are the closest analogs to the EMGs. Two of the high- z HCN detections (Cloverleaf and SMM J16359) lead to $L_{\text{FIR}}/L'_{\text{HCN}}$ values within the range expected from nearby galaxies, similar to the ratio in the best known ULIRG Arp 220 with $L_{\text{FIR}}/L'_{\text{HCN}} = 1340 L_{\odot} / \text{K km s}^{-1} \text{pc}^2$. The three other

detections have ratios about twice that of Arp 220. Only three of the 65 local galaxies have ratios in this range (2200 – 2600). Four measurements yield high upper limits to $L_{\text{FIR}}/L'_{\text{HCN}}$, outside the distribution expected from local galaxies including ULIRGs. There are also three weak upper limits that are not very useful. Combining the detections and upper limits, the star formation rate per solar mass of dense gas, measured by $L_{\text{FIR}}/L'_{\text{HCN}}$, is higher in EMGs than in the local Universe, including ULIRGs, by a factor of about 2.0 – 2.5.

It should be noted that with the exception of four SMGs, including the HCN detection reported here, all other EMGs in our sample host known AGN. Were the FIR luminosities of these EMGs to be corrected by the amount contributed by their AGN, the points plotted would, in principle, come into better agreement with the low- z correlation. However, for the three quasars where the corrections have been calculated (F10214+4724, Downes et al. 2004; Cloverleaf, Weiß et al. 2003; APM 08279+5255, (Weiß et al. 2005, 2007) the corrections are significant only for APM 08279, a highly luminous IR source with an unusual hot dust component (200K) connected with the QSO. Note, here we have used the rest frame FIR for all galaxies, local and high- z , instead of the IR luminosity that was used in GS04a for the local HCN sample.

Table 3 and Fig. 4 show that the ratio $L'_{\text{HCN}}/L'_{\text{CO}}$ for the EMGs is similar to that found in the local ULIRG population with the highest $L'_{\text{HCN}}/L'_{\text{CO}} = 0.27$ and an average of 0.19 (for 5 detections) compared with a maximum of 0.26 and an average of 0.13 for local ULIRGs. If we leave out APM 08279 the highest EMG value is 0.19 and the average is 0.13. Normal spiral galaxies have an average ratio of 0.03. Thus EMGs and ULIRGs have in common a high fraction of dense molecular gas compared to total molecular gas. All of the EMGs meet the luminous starburst criteria (Fig. 4) found by GS04a. Kohno (2005) claimed that nearby AGN tend to have exceptionally high HCN/CO ratios, presumably due to the X-ray dominated regions near AGN. But we did not find any similar cases in the AGN-dominated EMG sample at high- z as their HCN/CO ratios are comparable to that of local ULIRGs (Fig. 4). HCN observations of the local host galaxies of infrared-excess Palomar-Green QSOs also show that there is no evidence that the global HCN emission is enhanced relative to CO in galaxies hosting luminous AGN (Evans et al. 2006).

In conclusion we find that the EMGs have large quantities of dense molecular gas with HCN luminosities on average higher than local ULIRGs. They also have a high dense gas mass fraction, similar to ULIRGs. But, on average, they have a higher star formation rate per unit dense molecular gas than ULIRGs or local normal large spirals.

Significant progress requires the power of the Atacama Large Millimeter Array (ALMA), which will dramatically increase both the sample size and the quality of the measurements, to obtain rotational ladders, refine density estimates, and test other molecules such as HCO^+ ,

HNC, CS, etc., for measuring the physical properties of dense star-forming gas at high- z .

Yu Gao acknowledges the NRAO, particularly Chris Carilli, for hospitality shown. Support for this project came from NSF of China and Chinese Academy of Sci. (YG), and the Max-Planck Society (CC). CC and YG thank the Max-Planck Society and the Humboldt-Stiftung for partial support through the Max-Planck-Forschungspreis 2005.

REFERENCES

- Beelen, A., Cox, P., Benford, D.J. et al. 2006, *ApJ*, 642, 694
- Carilli, C.L., Solomon, P.M., Vanden Bout, P.A., et al. 2005, *ApJ*, 618, 586
- Downes, D., and Solomon, P.M. 2004, in preparation
- Egami, E., Neugebauer, G., Soifer, B.G., et al. 2000, *ApJ*, 535, 561
- Evans, A.S., Solomon, P.M., Tacconi, L.J., Vavilkin, T., Downes, D. 2006, *AJ*, 132, 2398
- Gao, Y., and Solomon, P.M., 2004a, *ApJ*, 606, 271 (GS04a)
- Gao, Y., and Solomon, P.M., 2004b, *ApJS*, 152, 63
- Greve, T.R., Hainline, L.J., Blain, A.W. et al. 2006, *AJ*, 132, 1938
- Isaak K., Chandler, C., and Carilli, C.L. 2004, *MNRAS*, 348, 1035
- Kneib, J.-P., Neri, R., Smail, I. et al. 2005, *A&A*, 434, 819
- Kohno, K. 2005, in “The Evolution of Starbursts: The 331st Wilhelm & Else Heraeus Seminar”, AIP Conference Proceedings, 783, 203 (astro-ph/0508420).
- Riechers, D.A., Walter, F., Carilli, C.R., et al. 2006, astro-ph/0606422
- Sanders, D.B., and Mirabel, I.F. 1996, *ARA&A*, 34, 749
- Solomon, P.M., Downes, D., and Radford, S.J.E. 1992, *ApJ*, 387, L55
- Solomon, P.M., Downes, D., & Radford, S.J.E., and Barrett, J.W. 1997, *ApJ*, 478, 144
- Solomon, P.M., Vanden Bout, P.A., Carilli, C.L., & Guélin, M. 2003, *Nature*, 356, 318
- Solomon, P.M. and Vanden Bout, P.A. 2005, *ARA&A*, 43, 677

Vanden Bout, P.A., Solomon., P.M., & Maddalena, R.J. 2004, ApJ, 614, 97
Wagg, J., Wilner, D.J., Neri, R., Downes, D., Wiklind, T. 2005, ApJ, 634, L13
Weiß, A., Henkel, C., Downes, D., Walter, F. 2003, A&A, 409, L41
Weiß, A., Downes, D., Walter, F., Henkel, C. 2005, A&A, 440, L45
Weiß, A., Downes, D., Neri, R., et al. 2007, astro-ph/0702669
Wu, J., Evans, N.J., Gao, Y. et al. 2005, ApJ, 635, L173

This preprint was prepared with the AAS L^AT_EX macros v5.0.

Table 1. Sources Observed

Source	z	R. A. (J2000)	Dec. (J2000)	t_{obs} (Hours)	ν_{obs} (GHz)
SMM J02396-0134	1.062	02:39:56.59	−01:34:26.6	21	43.0
SMM J04135+1027	2.846	04:13:27.50	+10:27:40.3	3	23.0
RX J0911.4+0551	2.796	09:11:27.50	+05:50:52.0	14	23.3
SMM J16359+6612	2.517	16:35:44.15	+66:12:24.0	16	25.2

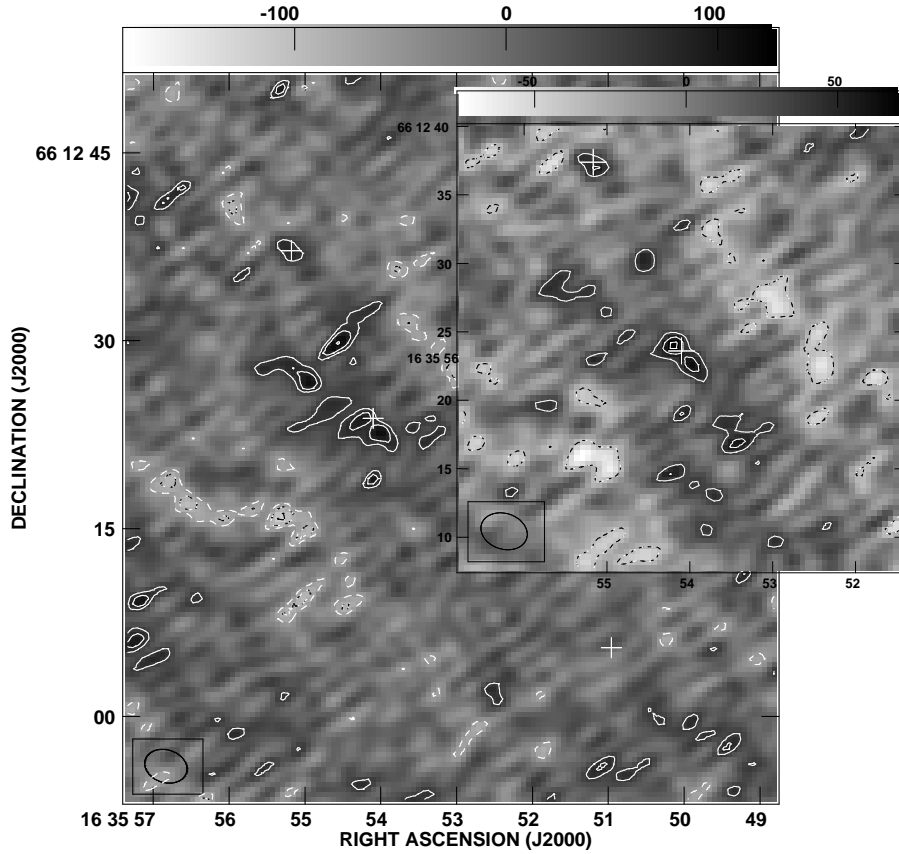


Fig. 1.— The larger image shows HCN emission from SMM J16359+6612, visible at the position of the CO component B (central cross: RA=16^h35^m54.^s1, DEC=66°12′23.″8). Contours plotted are -2.8, -2, 2, 2.8, and 4×12.7 mJy/beam km s⁻¹. The inset stacked image (see text) shows a $\sim 4\sigma$ detection at the CO component B. Contours plotted are -2, 2, 3, and 4×8mJy/beam km s⁻¹. Note the CO component A (NE cross) also shows possible HCN ($\sim 3\sigma$) detection.

Table 2. Observational Parameters and Results

Source	Beam FWHM (")	Noise ⁽¹⁾ (μ Jy/beam)	Ch. Width (MHz, km s ⁻¹)	$S_{\text{HCN}}\Delta v$ ⁽²⁾ (mJy km s ⁻¹)
SMM J02396-0134	2.0×1.7	105	50, 348.7	<73
	4.0×4.0	75		<92
SMM J04135+10277	3.5×3.1	76	3.1, 40.6	<63
RX J0911.4+0551	3.7×3.3	62	3.1, 40.1	<29
SMM J16359+6612	3.0×2.5	96	3.1, 37.2	33

¹The root-mean-square noise in the channel maps.

²Upper limits (3σ in moment zero maps) are 3 times integrations of the noise over the frequency channels where the HCN line was expected from observed CO lines.

Table 3. Intrinsic Properties from HCN (1-0) Detections and Upper Limits*

Source	$L_{\text{FIR}}/L'_{\text{HCN}}$ (L_{\odot}/L_l^{\dagger})	L_{FIR} ($10^{12} L_{\odot}$)	L'_{HCN} ($10^9 L_l^{\dagger}$)	L'_{CO}	$L'_{\text{HCN}}/L'_{\text{CO}}$	Lens Mag.	Refs. [‡]
VCV J1409+5628	2570	17	6.5	74	0.09	1	2, 3, 4
APM 08279+5255	1000	0.25	0.25	0.92	0.27	80	5, 6, 7
H1413 (Cloverleaf)	1690	5.0	3.0	37	0.08	11	4
IRAS F10214+4724	2770	3.4	1.2	6.5	0.18	17	4, 8
J16359+6612(B)	1430	0.93	0.6	3.7	0.18	22	1, 4
BR 1202-0725	>1405	55	<39	93	<0.42	1	9, 10
SMM J04135+1027	>800	22	<28	159	<0.18	1.3	1, 4
SMM J02399-0136	>609	28	<46	112	<0.41	2.5	4, 11
SDSS J1148+5251	>2200	20	<9.3	25	<0.36	1	2, 3, 4
SMM J02396-0134	>1625	6.1	<3.7	19	<0.20	2.5	1, 4
SMM J14011+0252	>2500	0.7-3.7	<0.3-1.5	4-18	<0.08	25-5	3, 4
MG0751+2716	>2900	2.7	<0.9	9.3	<0.10	17	3, 4
RX J0911+0551	>3280	2.1	<0.6	4.8	<0.13	22	1, 4

*Calculated using $H_0 = 75 \text{ km s}^{-1} \text{ Mpc}^{-1}$, $\Omega_{\Lambda} = 0.7$, $\Omega_m = 0.3$, and lens magnifications listed.

[†] $L_l = K \text{ km s}^{-1} \text{ pc}^2$.

[‡]References – (1) This paper; (2) Beelen et al. (2006); (3) Carilli et al. (2005); (4) Solomon and Vanden Bout (2005); (5) We adopt the Weiß et al. (2007) detailed two component model of the CO and HCN excitation and use the predicted HCN(1-0) and FIR luminosity from the collisionally excited gas in the dense cold (65K) star forming component. The observed HCN(5-4) line is produced by the unusually hot dust at $T = 200\text{K}$; (6) Wagg et al. (2005); (7) Egami et al. (2000); (8) Downes and Solomon (2004); (9) Riechers et al. (2006); (10) Isaak et al. (2004); (11) Greve et al. (2006).

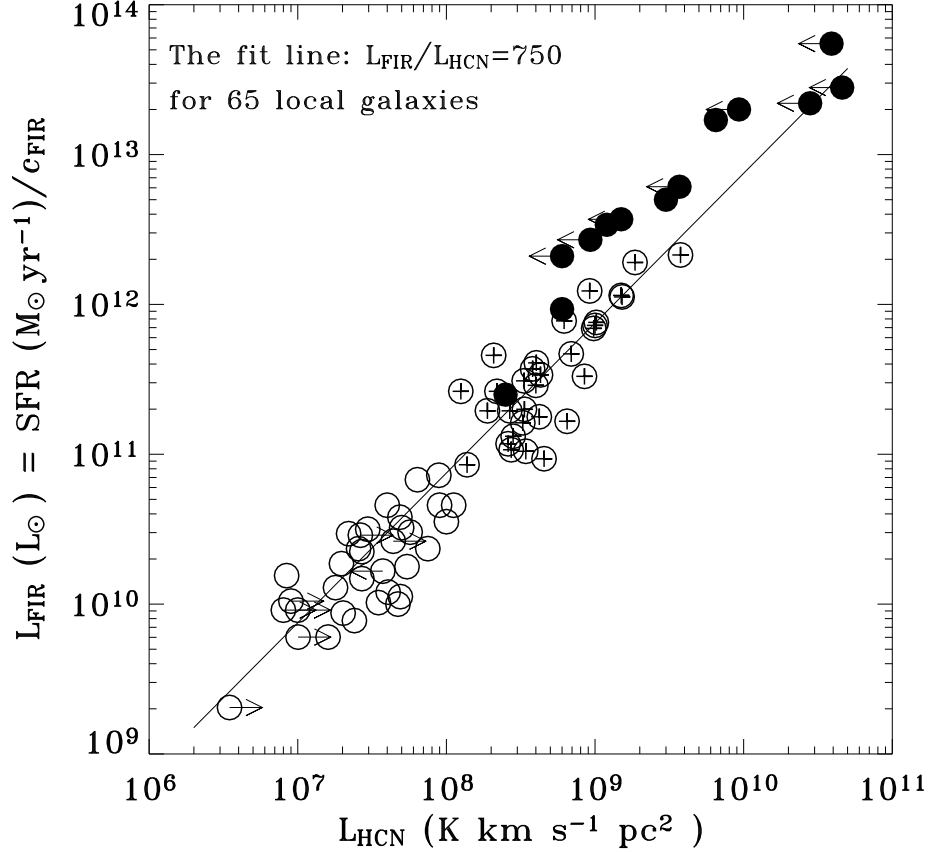


Fig. 2.— The correlation between HCN and FIR luminosities in 13 EMGs and 65 local galaxies (GS04a, note FIR is used here). The high- z EMGs are indicated in solid circles, local LIRGs and ULIRGs in crosses, and normal spirals in open circle. Limits in HCN luminosities are indicated with arrows. The line is the fit to the entire 65 local galaxies with a slope fixed at unity (same as the formal slope of the fit: 0.99). Note that the local LIRGs and ULIRGs fit this line but the EMGs lie above the line by a factor of 2–2.5 indicating a higher star formation rate per solar mass of **dense** molecular gas.

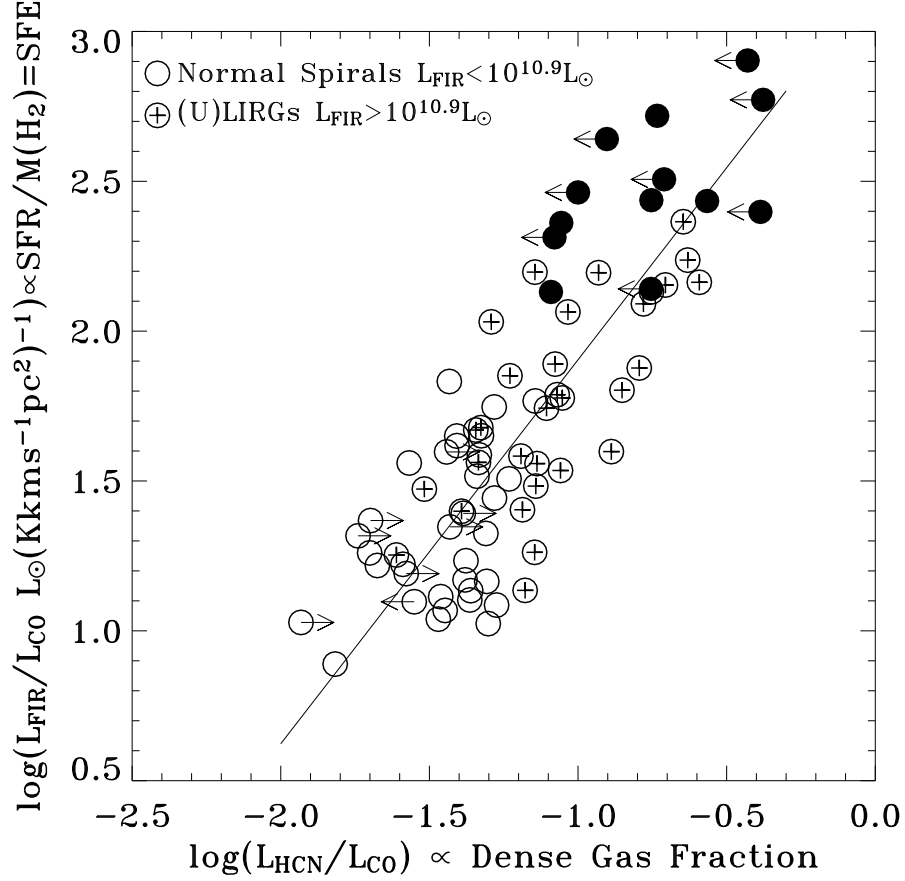


Fig. 3.— Correlation between $L_{\text{HCN}}/L_{\text{CO}}$ and $L_{\text{FIR}}/L_{\text{CO}}$ revealing the physical relationship between the HCN and FIR since both luminosities are normalized by L'_{CO} , removing the dependence on distance and galaxy size. The line is the best fit for the local sample of GS04a. The high- z EMGs (solid circles) show some FIR/CO excess.

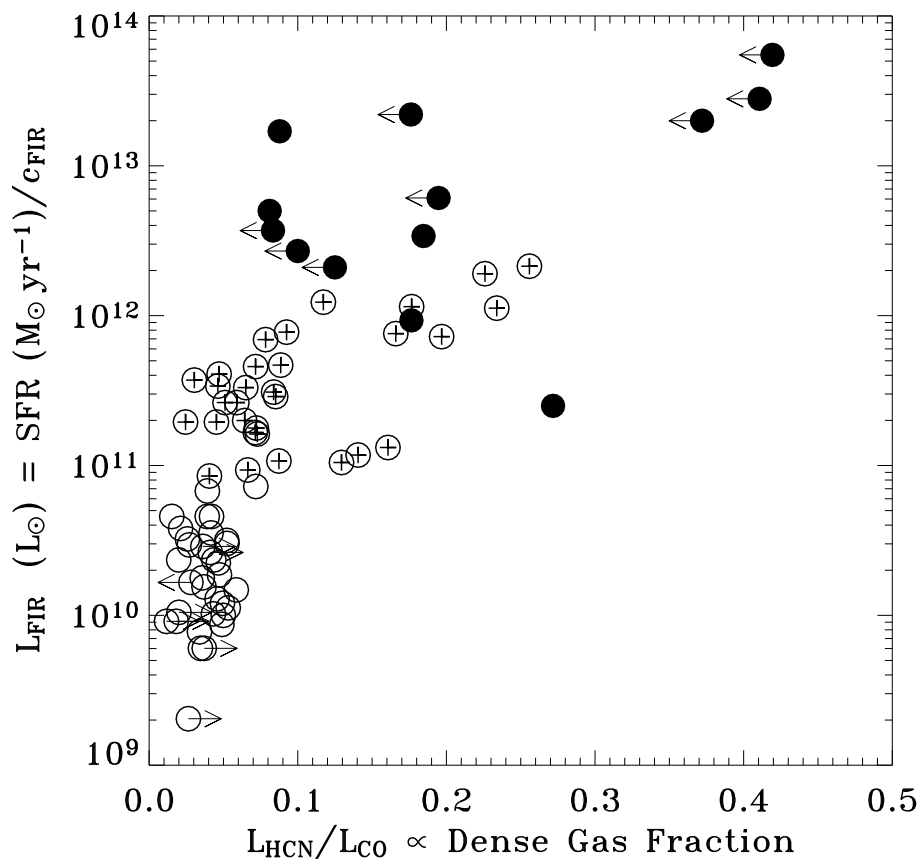


Fig. 4.— L_{FIR} vs. $L_{\text{HCN}}/L_{\text{CO}}$. All galaxies with a high dense molecular gas fraction of $L_{\text{HCN}}/L_{\text{CO}} > 0.06$, whether local or high- z , are IR-luminous ($L_{\text{FIR}} > 10^{11} L_{\odot}$). The high- z EMGs are indicated in solid circles, local LIRGs and ULIRGs in crosses, and normal spirals in open circles. The high- z EMGs show a high ratio of dense to total molecular gas similar to ULIRGs but even higher FIR luminosity.